99-12

E1-99-12

Y.A.Kulchitsky*, V.B.Vinogradov

NON-COMPENSATION OF THE ATLAS BARREL
TILE HADRON MODULE-0 CALORIMETER

*On leave from: Institute of Physics, National Academy of Sciences, Minsk, Belarus

1999

Кульчицкий Ю.А., Виноградов В.Б.

E1-99-12

Нескомпенсированность модуля-0
адронного цилиндрического калориметра установки АТЛАС

Представлена детальная экспериментальная информация об энерговыделении электронов и пионов, энергетическом разрешении электронов и *elh*-отношении в зависимости от энергии пучка, Z-координаты и угла входа налетающей частицы в модуле-0 Fe-сцинтилляционного цилиндрического адронного калориметра с продольным расположением сцинтилляционных пластин установки АТЛАС. Эти результаты основаны на данных, полученных в 1996 г. при экспонировании калориметра в электронных и адронных пучках с энергиями 10−180 ГэВ ускорителя SPS в ЦЕРН. Результаты сравниваются с существующими экспериментальными данными для однометровых модулей прототипа калориметра и с данными для различных Fe-сцинтилляционных калориметров, а также с расчетами методом Монте-Карло.

Работа выполнена в Лаборатории ядерных проблем ОИЯИ.

Kulchitsky Y.A., Vinogradov V.B.

E1-99-12

Non-Compensation
of the ATLAS Barrel Tile Hadron Module-0 Calorimeter

The detailed experimental information about the electron and pion responses, the electron energy resolution and the *elh* ratio as a function of incident energy E, impact point Z and incidence angle Θ of the Module-0 of the ATLAS iron-scintillator barrel hadron calorimeter with the longitudinal tile configuration is presented. The results are based on the electron and pion beams data for $E = 10, 20, 60, 80, 100$ and 180 GeV at $\eta = -0.25$ and -055, which have been obtained during the test beam period in 1996. The results are compared with the exciting experimental data of TILECAL 1m prototype modules, various iron-scintillator calorimeters and with some Monte Carlo calculations.

The investigation has been performed at the Laboratory of Nuclear Problems, JINR.

1 Introduction

The ATLAS Collaboration is building a general-purpose pp detector which is designed to exploit the full discovery potential of the CERN's Large Hadron Collider (LHC), a super-conducting ring to provide proton – proton collisions around 14 TeV [1]. LHC will open up new physics horizons, probing interactions between proton constituents at the 1 TeV level, where new behavior is expected to reveal key insights into the underlying mechanisms of Nature [2].

The bulk of the hadronic calorimetry in the ATLAS detector is provided by a large (11 m in length, 8.5 m in outer diameter, 2 m in thickness, 10000 readout channels) scintillating tile hadronic barrel calorimeter (TILECAL). The technology for this calorimeter is based on a sampling technique using steel absorber material and scintillating plates readout by wavelength shifting fibres. An innovative feature of this design is the orientation of the scintillating tiles which are placed in planes perpendicular to the colliding beams staggered in depth [3] (Fig. 1).

In order to test this concept five 1m prototype modules and the Module-0 were built and exposed to high energy pion, electron and muon beams at the CERN Super Proton Synchrotron.

In the following we consider two test beam setups. The setup 1, shown in Fig. 3-1 given in [4], consists of five 1m prototype modules. The obtained results about the electron and pion responses and the e/h ratio [5] for this setup are used in this paper for comparison. The setup in question (setup 2), shown in Fig. 3-2 given in [4], has as the basis Module-0.

In this work the detailed experimental information is presented about the electron and pion responses and the e/π and e/h ratios (an intrinsic non-compensation) of the Tile calorimeter Module-0.

2 The 1m Prototype Modules

Each module spans 100 cm in the Z direction, 180 cm in the X direction (about 9 interaction lengths at $\eta = 0$ or about 80 effective radiation lengths) and with a front face of 100×20 cm^2 [6]. The iron structure of each module consists of 57 repeated "periods". Each period is 18 mm thick and consists of four layers. The first and third layers are formed by large trapezoidal steel plates (master plates), and spanning the full
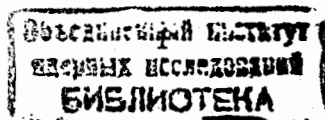
longitudinal dimension of the module. In the second and fourth layers, smaller trapezoidal steel plates (spacer plates) and scintillator tiles alternate along the X direction. These layers consist of 18 different trapezoids of steel or scintillator, each spanning 100 mm along X.

The master plates, spacer plates and scintillator tiles are 5 mm, 4 mm and 3 mm thick, respectively. The iron to scintillator ratio is 4.67:1 by volume.

Wavelength shifting fibres collect scintillation light from the tiles at both of their open edges and bring it to photo-multipliers (PMTs) at the periphery of the calorimeter. Each PMT views a specific group of tiles through the corresponding bundle of fibres.

The modules are longitudinally segmented into four depth segments by grouping fibers from different tiles. As a result, each module is divided into 5 (*along Z*) × 4 (*along X*) separate cells. The readout cells have the lateral dimensions 200 mm (*along Z*) × (200 − 380) mm (along Y, depending on a depth number) and the longitudinal dimensions 300, 400, 500, 600 mm for depths 1 − 4, corresponding to 1.5, 2, 2.5 and 3 λ_I at $\eta = 0$. At the output we have 200 values of responses Q_{ijkl} from PMT properly calibrated [6] with pedestal subtracted, for each event. Here $i = 1, \ldots, 5$ is the column of cells (tower) number, $j = 1, \ldots, 5$ is the module number, $k = 1, \ldots, 4$ is the depth number and $l = 1, 2$ is the PMT number.

3   The Module-0

The layout of the readout cell geometry for the Module-0 is shown in Fig. 3-3 given in [4]. The Module-0 has three depth segmentations. The thickness of the Module-0 at $\Theta = 0°$ is 1.5 λ in the first depth sampling, 4.2 λ in the second and 1.9 λ in the third with a total depth of 7.6 λ. The Module-0 samples the shower with 11 tiles varying in depth from 97 to 187 mm. The front face area is of 560×22 cm^2.

In the setup 2 (see Fig.3-2 given in [4]) the 1m prototype modules are placed on a scanning table on top and at the bottom of the Module-0 with a 10 cm gap between them. This scanning table allowed movement in any direction. Upstream of the calorimeter, a trigger counter telescope (S1-S3) was installed, defining a beam spot of 2 cm in diameter. Two delay-line wire chambers (BC1-BC2), each with Z, Y readout, allowed the impact point of beam particles on the calorimeter face to be reconstructed

to better than ±1 mm [7]. A helium Čerenkov threshold counter was used to tag π-mesons and electrons for E =10 and 20 GeV. For the measurements of the hadronic shower longitudinal and lateral leakages back ($80 \times 80 cm^2$) and side ($40 \times 115 cm^2$) "muon walls" were placed behind and on the side of the calorimeter.

4   Data Taking and Event Selection

Data were taken with electron and pion beam of E = 10, 20, 60, 80, 100 and 180 GeV at $\eta = -0.25$ and −0.55, The following 6 cuts were used. The cuts 1 and 2 removed beam halo. The cut 3 removed muons and non-single-track events. The cuts 4, 5 and 6 carried out the electron-pion separation The cut 4 is connected with Čerenkov counter amplitude. Cut 5 is the relative shower energy deposition in the first two calorimeter depths:

$$C_i = \sum_{selected\ i} \sum_{j=3} \sum_{k=1}^{2} \sum_{l=1}^{2} Q_{ijkl}/E, \qquad (1)$$

where

$$E = \sum_{ijkl} Q_{ijkl}. \qquad (2)$$

and the indexes i and k in Q_{ijkl} determine the regions of electromagnetic shower development. The values C_i depend on a particle's entry angle Θ. The basis for the electron-hadron separation by using the cut 5 is the very different longitudinal energy deposition for electrons and hadrons.

The cut 6 is related with the lateral shower spread [8]:

$$E_{cut} = \frac{\sqrt{\sum_c (E_c^\alpha - \sum_c E_c^\alpha/N_{cell})^2}}{\sum_c E_c^\alpha}, \qquad (3)$$

where $1 \leq c \leq N_{cell}$ and N_{cell} is the used cells number. The power parameter $\alpha = 0.6$ have been tuned in [8] to achieve maximum separation efficiency.

The distributions of events as a function of C_i and E_{cut} for various energies at $\eta = -0.25$ and $\eta = -0.55$ are shown in Fig. 2 and Fig. 3. Fig. 4 shows the scatter plots E_{cut} versus C_i. Two groups of events are clearly separated: the left group corresponds to pions, the right group corresponds to electrons.

5 Electrons Response

As to the electron response our calorimeter is very complicated object. It may be imagined as a continuous set of calorimeters with the variable absorber and scintillator thicknesses (from $t = 58$ to 28 mm and from $s = 12$ to 6 mm for $14^o \leq \Theta \leq 30^o$), where t and s are the thicknesses of absorber and scintillator respectively.

Therefore an electron response ($R = E_e/E_{beam}$) is rather complicated function of E_{beam}, Θ and Z. The energy response spectrum for given run (beam has the transversal spread ± 10 mm) as a rule is non-Gaussian (Fig. 5 and Fig. 6), since it is a superposition of different response spectra, but it becomes Gaussian for given E, Θ, Z values. Fig. 7 and Fig. 8 show the normalized electron response for E = 10, 20, 60, 80, 100, 180 GeV at $\eta = -0.25$ and -0.55 as a function of the impact point Z coordinate. One can see the clear periodical structure of the response with 18 mm period. The mean values (parameter P_2) and the amplitudes(parameter P_1) of these spectra have been extracted by fitting the sine function:

$$f(Z) = P_2 + P_1 \sin\left(2\pi Z/P_3 + P_4\right). \tag{4}$$

Fig. 9 (top) shows the parameter P_1 as a function of the beam energy. As can be seen this parameter does not depend from the beam energy within errors and decreases with increasing of η from $(7.6 \pm 0.3)\%$ at $\eta = -0.25$ to $(2.9 \pm 0.2)\%$ at $\eta = -0.55$.

Fig. 9 (bottom) shows the mean normalized electron response as a function of energy for two values of η. As can be seen there is some increase of the mean normalized electron response with increasing of energy. There is no difference between ones for various values of η. Note that there are the additional systematic errors in these values (not given in this Figure) due to the uncertainties in the average beam energies. These uncertainties are determined by the expression

$$\frac{\Delta E_{beam}}{E_{beam}} = \frac{25\%}{E_{beam}} \oplus 0.5\%$$

and range from 2.5 % for $E_{beam} = 10$ GeV to 0.5 % for $E_{beam} = 180$ GeV.

We attempted to explain the electron response as a function of Z coordinate calculating the total number of shower electrons (positrons) crossing scintillator tiles taking into account the arrangement of tiles and its sizes and using the shower curve (the number of particles in the shower N_e as a function of the longitudinal shower development). which is given in [9]. These calculations were performed for some energies and angles for the trajectories entering into four different elements of calorimeter periodic structure — spacer, master, tile, master. The results for E = 10, 100, 180 GeV at $\eta = -0.25$ are shown in Fig. 10. There is a maximum at the impact point corresponding to tile and a minimum at the spacer plate. Such simple calculations are in agreement with experimental data as to non-dependence from energy and the periodicity in the electron response. But these calculations do not reproduce the values of the amplitude. The latter is connected with non-taking into account the shower lateral spread.

6 Electron Energy Resolution

The relative electron energy resolutions, extracted from the energy distributions (Fig. 5 and Fig. 6), are shown in Fig. 11 together with the 1m prototype data as a function of $1/\sqrt{E}$. Fit of these data by the expression (5) produced the parameters a_{exp} and b_{exp} given in Table 1 together with the data for various iron-scintillator calorimeters.

$$\frac{\sigma}{E} = \frac{a}{\sqrt{E}} \oplus b, \tag{5}$$

We compared our results on the energy resolution with the parameterization suggested in [10]:

$$\frac{\sigma}{E} = \frac{a}{\sqrt{E}} = \frac{\sigma_o}{\sqrt{E}} \cdot \left(\frac{t}{X_t}\right)^{\gamma} \cdot \left(\frac{s}{X_s}\right)^{-\delta}, \tag{6}$$

where $\sigma_o = 6.33\ \% \cdot \sqrt{GeV}$, $\gamma = 0.62$, $\delta = 0.21$ are the parameters, X_t and X_s are the radiation lengths of iron and scintillator respectively. In our case the values of t and s are equal to: $t = 14\ mm/\sin\Theta$, $s = 3\ mm/\sin\Theta$. This formula is purely empirical and the parameters σ_o, γ, δ were determined by fitting the Monte Carlo data.

The results of calculations are given in Table 1. As can be seen from this Table the energy resolutions obtained for "ideal" calorimeter are more accurate (about a factor 1.5) than the experimental ones.

7 Pion Response

Fig. 12 shows the normalized pion response (E_π E_{beam}) for $E_{beam} = 20$, 100, 180 GeV at $\eta = -0.25$ and -0.55. Fig. 13 shows the normalized pion response for $E_{beam} = 20$, 100, 180 GeV at $\eta = -0.25$ and -0.55 as a function of impact point Z coordinate. Contrary to electrons these pion Z-dependences do not show any significant periodical structure.

Fig. 17 shows the mean normalized pion response, extracted from Fig. 13, as a function of energy for two values of η. The meaning of lines is given below. As can be expected, since the e/π ratio is not equal to 1, the mean normalized pion response increases with the beam energy increasing.

As can be seen the pion response is different for various η. The values of the pion response for $\eta = -0.55$ are larger than ones for $\eta = -0.25$. We tried to explain if the reason of this difference is the lateral leakage through gaps between the 1m prototype modules. We estimated the lateral leakages to the gaps taking into account the longitudinal energy deposition and the spatial radial deposition. It turned out that the leakage for $\eta = -0.25$ is larger than for $\eta = -0.55$ but it is unsufficient, less than 1 %, in order to explain the observed difference in the pion responses.

8 e/h Ratio

The responses obtained for e and π give the possibility to determine the e/h ratio, an intrinsic non-compensation of a calorimeter. In our case the electron – pion ratios reveal complicated structures $e/\pi = f(E, \Theta, Z)$. Fig. 14 and Fig. 15 show the e/π ratios for Module-0 for E = 10, 20, 60, 80, 100 and 180 GeV at $\eta = -0.25$ and -0.55 as a function of Z coordinate. If for the 1m prototype modules the local compensation has been observed (for some Z points at 20 GeV and $\Theta = 10^o$, see Fig. 4 given in [5]) as to the Module-0 this is not this case.

The e/π ratios, averaged over two 18 mm period, are shown in Fig. 16 as a function of the beam energy. The errors include statistical errors and a systematic error of 1 %, added in quadrature.

For extracting the e/h ratio we have used two methods: the standard e/π method and the pion response method.

In the first method, the relation between the e/h ratio and the e/π ratio is:

$$e/\pi = \frac{<E_e>}{<E_\pi>} = \frac{e/h}{1 + (e/h - 1) \cdot f_{\pi^0}}, \qquad (7)$$

where f_{π^0} is the average fraction of the energy of the incident hadron going into π^0 production [12].

In the second method, the relation between the e/h ratio and the pion response, $<E_\pi>$, is:

$$\frac{<E_\pi>}{E_{beam}} = \frac{e}{e/h}(1 + (e/h - 1) \cdot f_{\pi^0}), \qquad (8)$$

where e is the efficiency for the electron detecting. Note that usually this is two parameters fit [8] with parameters e and e/h. In principle, the e value can be determined from the ratio $e = <E_e>/E_{beam}$.

There are two analytic forms for the intrinsic π^o fraction suggested by Groom [11]

$$f_{\pi^o} = 1 - \left(\frac{E}{E'_o}\right)^{m-1} \qquad (9)$$

and Wigmans [12]

$$f_{\pi^o} = k \cdot ln\left(\frac{E}{E'_o}\right), \qquad (10)$$

where $E'_o = 1$ GeV, $m = 0.85$, $k = 0.11$.

We used both parameterizations. Fig. 16 shows the e/π ratio as a function of the beam energy for Module-0 and its fitting of equation (7) with the Wigmans (Groom) parameterization of $f_{\pi^o}(E)$.

Fig. 17 shows the pion response as a function of the beam energy for the Module-0 and its fitting of equation (8) with the Wigmans (solid line) and Groom (dashed line) parameterizations of $f_{\pi^o}(E)$.

The confidence levels of the fits for these parameterizations are good, i.e., χ^2 is less then the numbers of degrees of freedom. So, we could obtain four values for the e/h ratio. The results are presented in Table 2.

As can be seen, the e/h ratios obtained by the pion response method have the errors about 10 times larger than obtained by the e/π method. In addition, there is some systematic difference: the e/h ratios, obtained by the pion response method, are of 20 – 40 % larger than ones, obtained by the e/π method. This can be explained by some increase in the electron response in the 60 – 180 GeV energy range. This systematic

is cancelled in the e/π method. It is remarkable that in [8], in which the e/h ratio for the 1m prototype modules have been determined, obtained the contrary result concerning advantages in using these methods. Advantage have been observed for the pion response method. In their case the standard e/π method led to a larger error (about a factor 2) than the pion response method called in this work the non-linearity method. This can be explained by different scale of errors in the corresponding input data. In their work the e/π ratios had 3 % errors and the pion response values had 0.3 % errors. In our case, errors in the e/π ratios and the pion response values have errors at the same 1 % level.

We made preference to the e/π method and our final results are: $e/h = 1.45 \pm 0.014$ for $\eta = -0.25$ and $e/h = 1.36 \pm 0.014$ for $\eta = -0.55$. Fig. 18 shows these values together with ones for the 1m prototype modules as a function of Θ angle. The difference in Θ behavior is observed. This can be explained by different behaviour for the electron and pion responses as a function of Θ for these two calorimeters as shown in Fig. 19. For the Module-0 it is observed slight decrease of the electron response and some increase of the pion response. As a result of the e/h ratio has 6 % decrease.

The simple calculations of the responses by counting of the energy depositions in crossing tiles along the shower axes taking into account the arrangement and sizes of tiles and the longitudinal shower profiles confirmed these observations.

The obtained e/h values are given in Table 3 with the other existing experimental data and the Monte Carlo calculations for various iron-scintillator calorimeters. The corresponding values of the thickness of the iron absorber (t), the thickness of the readout scintillator layers (s), the ratio $R_d = t/s$ and the used symbols are also given. These e/h values are also shown in Fig. 20 as a function of R_d ratio and the iron thickness. As can be seen the e/h ratio has very complicated behaviour being the function of the thickness of the passive (iron) layers, the sampling fraction and, in our case, from the Θ angle and the sizes and replacement of the scintillator tiles.

Besides, the considerable disagreement between different Monte Carlo calculations [13], [14] and experimental data is observed.

Table 1: The values of parameter a_{exp} and b_{exp} of the electron energy resolution for various iron-scintillator calorimeters. a_{th} is the prediction of the parameterization of Del Peso et al.

Author	Ref.	t	s	a_{exp}	b_{exp}	a_{th}
Stone	[15]	4.8	6.3	10.		7.0
Antipov	[16]	20.	5.0	27.		17.
Abramovicz	[17]	25.	5.0	23.		20.
Mod.0, 30°		28.	6.0	33. $\pm$ 2.	1. $\pm$ 0.3	20.
1m pr., 30°	[5]	28.	6.0	33. $\pm$ 9.	0.1 $\pm$ 0.8	20.
1m pr., 20°	[5]	41.	9.	36. $\pm$ 5.	0.8 $\pm$ 5.0	20.
Mod.0, 14°		58.	12.0	32. $\pm$ 4.	2.5 $\pm$ 0.5	27.
1m pr., 10°	[5]	81.	17.	58. $\pm$ 4.	1.4 $\pm$ 0.4	32.

Table 2: The values of the e/h ratio for different methods and $f_{\pi^o}(E)$ parameterizations (W – the Wigmans parameterization, G – the Groom parameterization).

Method	$f_{\pi^o}(E)$	e/h	
		$\eta = -0.25$	$\eta = -0.55$
e/π	W	1.45$\pm$0.014	1.35$\pm$0.013
	G	1.45$\pm$0.015	1.36$\pm$0.013
π	W	1.72$\pm$0.11	1.56$\pm$0.07
	G	2.00$\pm$0.19	1.76$\pm$0.11

Table 3: The e/h ratios for our and various iron-scintillator calorimeters. t is the thickness of the iron absorber, s is the thickness of the readout scintillator layers and the ratio $R_d = t/s$.

Author	Ref.	R_d	t, mm	s, mm	e/h	Symb.
Bohmer	[18] **	2.8	20.	7.0	1.44±0.03	○
Wigmans	[13] *	3.0	15.	5.0	1.25	▲
Wigmans	[13] *	4.0	20.	5.0	1.23	▲
Module-0, 30°		4.7	28.	6.0	1.36 ± 0.014	▣
1m prot., 30°	[5]	4.7	28.	6.0	1.39 ± 0.03	□
1m prot., 20°	[5]	4.7	41.	9.0	1.34 ± 0.03	□
Module-0, 14°		4.7	58.	12.	1.45 ± 0.014	■
1m prot., 10°	[5]	4.7	81.	17.	1.23 ± 0.02	□
Wigmans	[13] *	5.0	25.	5.0	1.21	▲
Abramovicz	[17] **	5.0	25.	5.0	1.32±0.03	◇
Vincenzi	[19] **	5.0	25.	5.0	1.32±0.03	★
Wigmans	[13] *	6.0	30.	5.0	1.20	▲
Gabriel	[14] *	6.3	19.	3.0	1.55	▼
Wigmans	[13] *	8.0	40.	5.0	1.18	▲
Holder	[20] **	8.3	50.	6.0	1.18±0.02	∗
Gabriel	[14] *	8.5	25.4	3.0	1.50	▼
Wigmans	[13] *	10.	50.	5.0	1.16	▲

* Monte Carlo calculations

** The our estimate of 2 % error is given
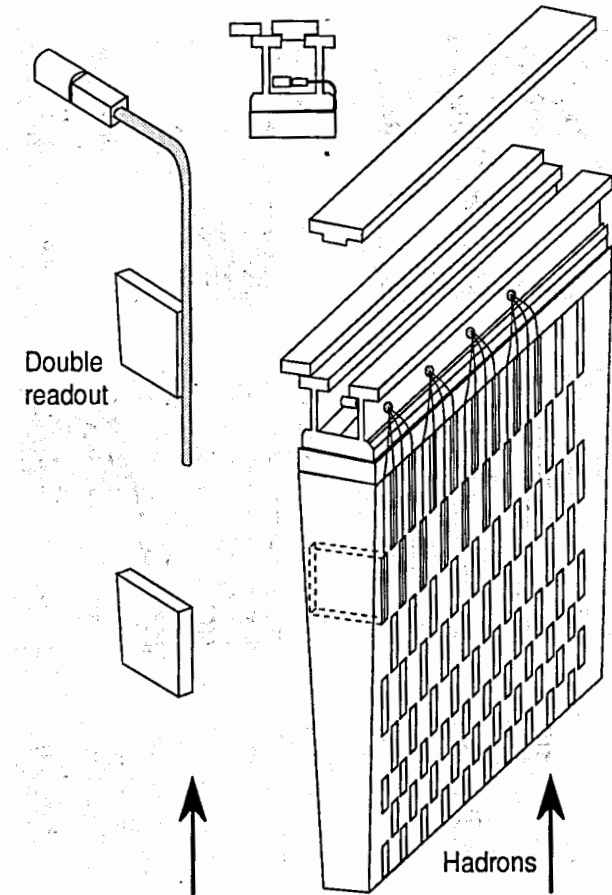
Figure 1: Principle of the tile hadronic calorimeter.
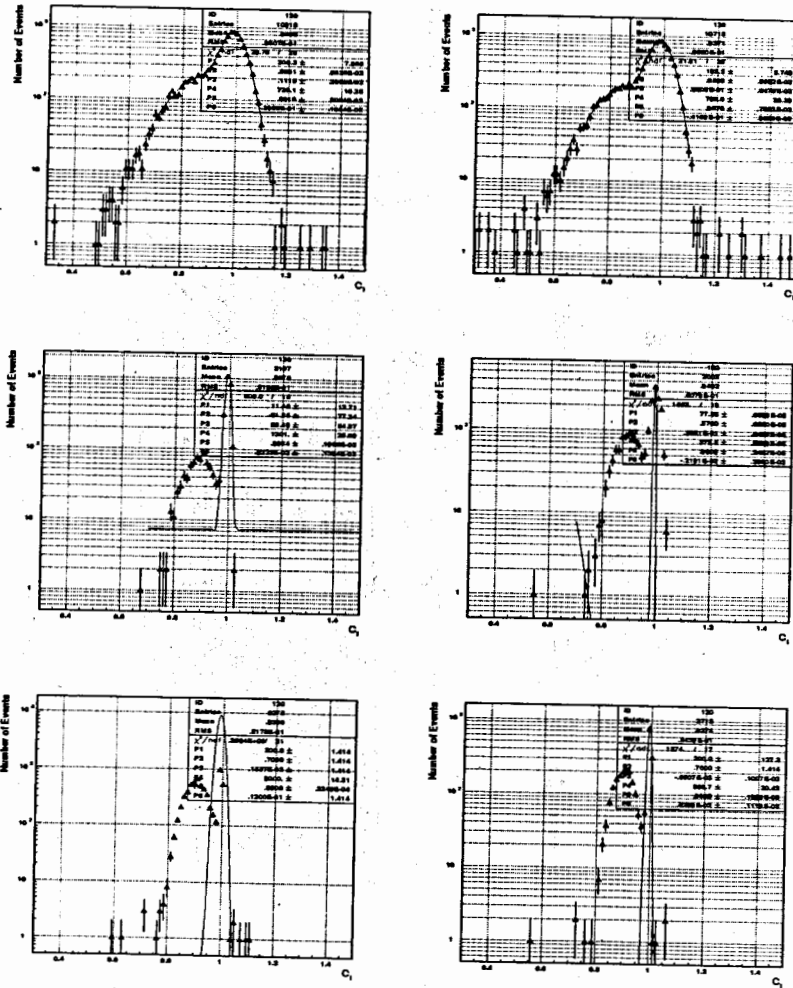
Figure 2: The distributions of the events as a function of C_i for for E = 20, 100, 180 GeV at $\eta = -0.25$ (left column, up to down) and at $\eta = -0.55$ (right column, up to down).
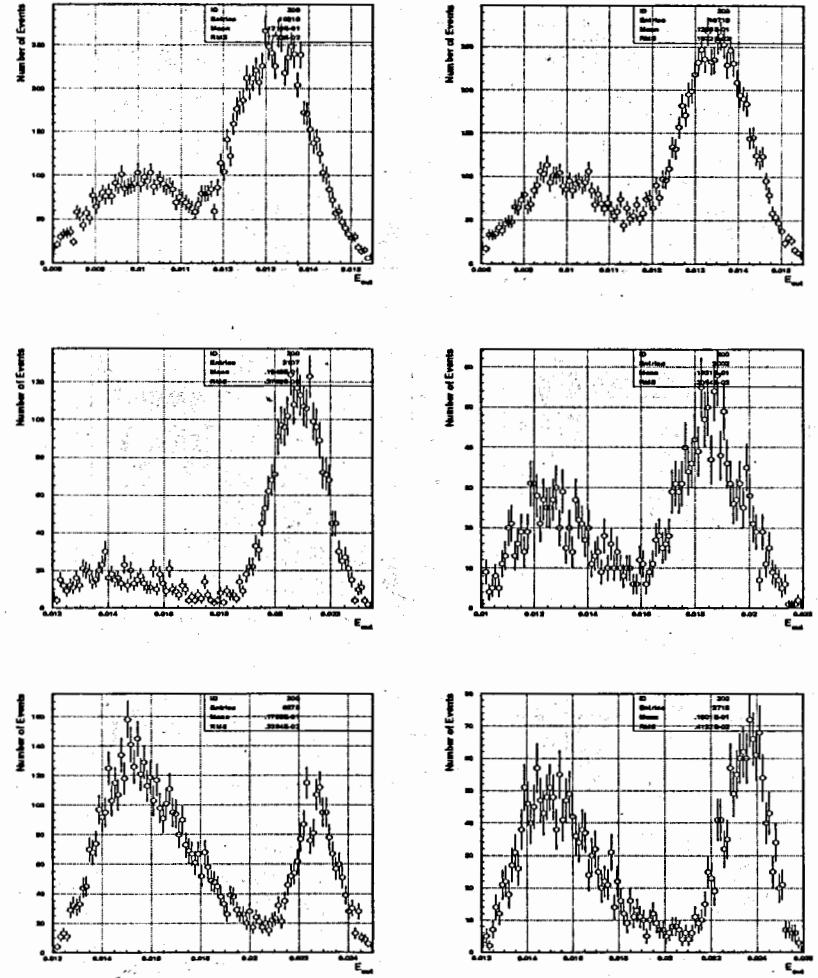
Figure 3: The distributions of the events as a function of E_{cut} for E = 20, 100, 180 GeV at $\eta = -0.25$ (left column, up to down) and at $\eta = -0.55$ (right column, up to down).
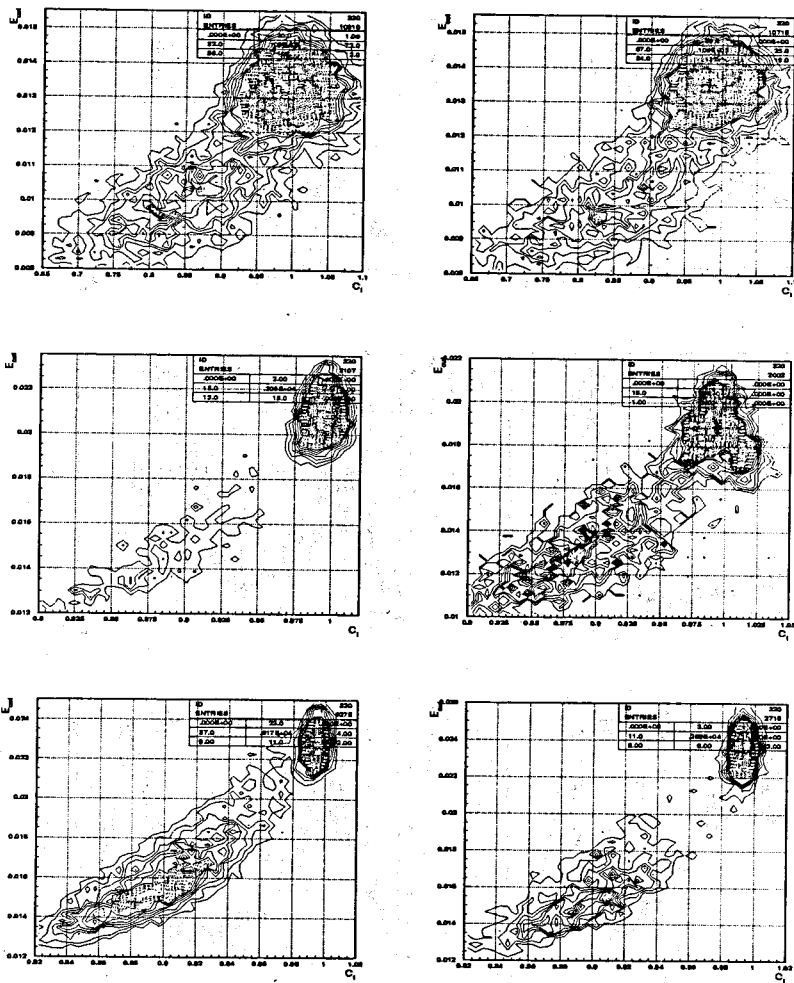
Figure 4: The scatter plots E_{cut} versus C_i for E = 20, 100, 180 GeV at $\eta = -0.25$ (left column, up to down) and at $\eta = -0.55$ (right column, up to down).
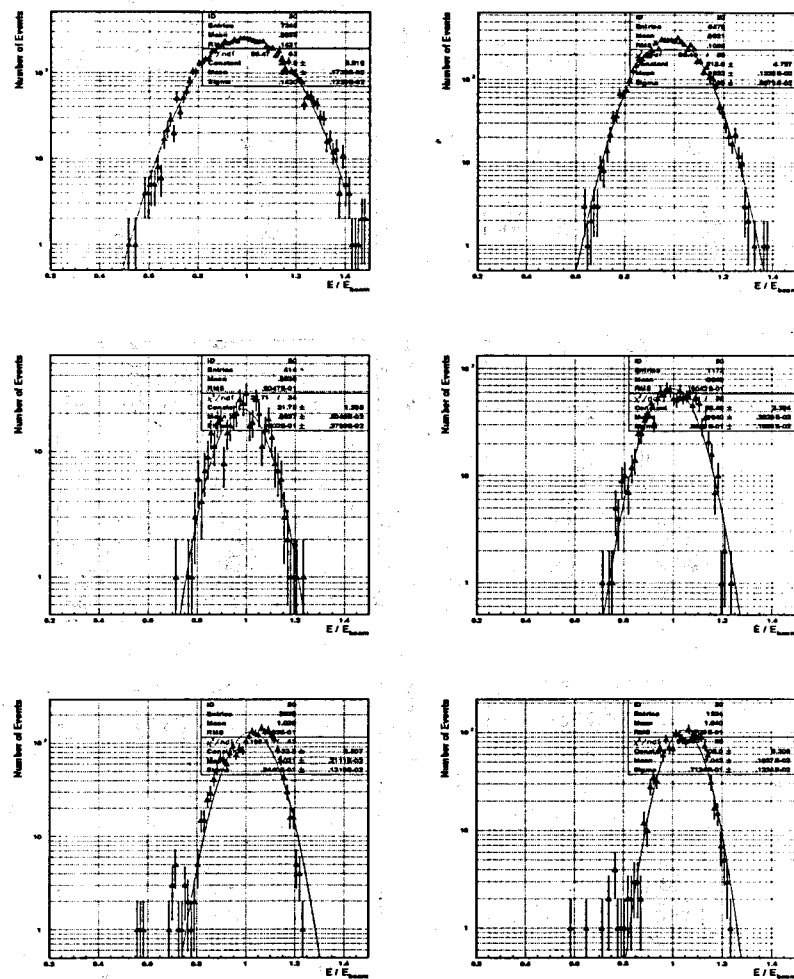
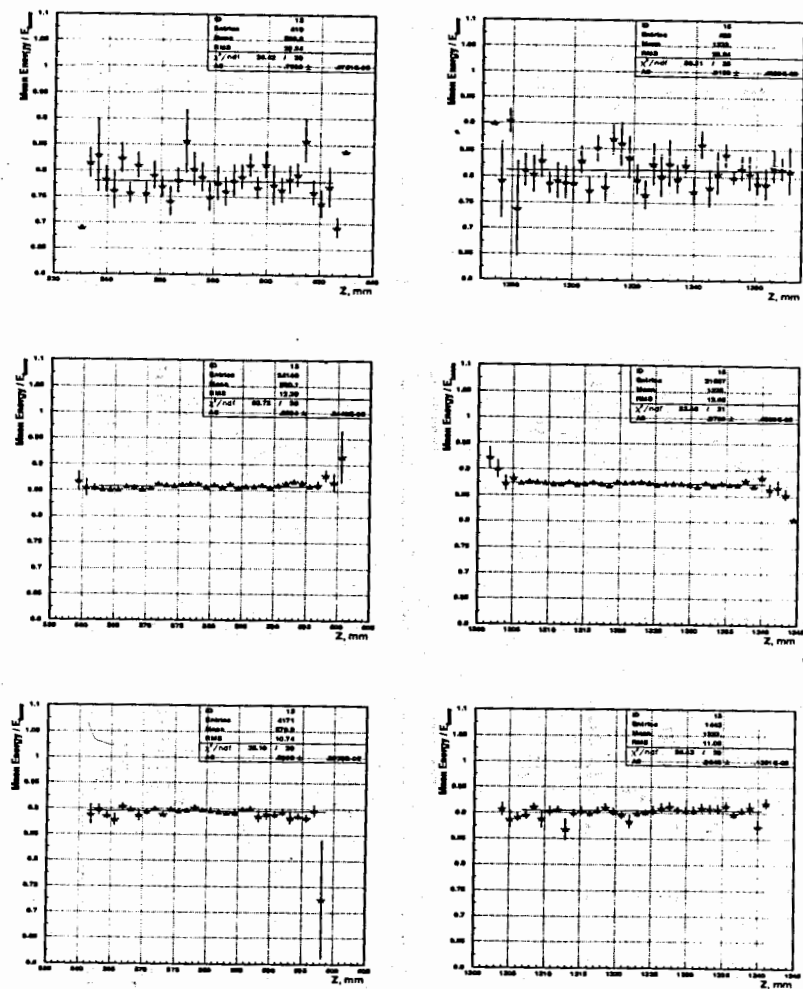Figure 5: The normalized electron response (E_e/E_{beam}) for E = 10, 60, 100 GeV (left column, up to down) and E = 20, 80, 180 GeV (right column, up to down) at $\eta = -0.25$.
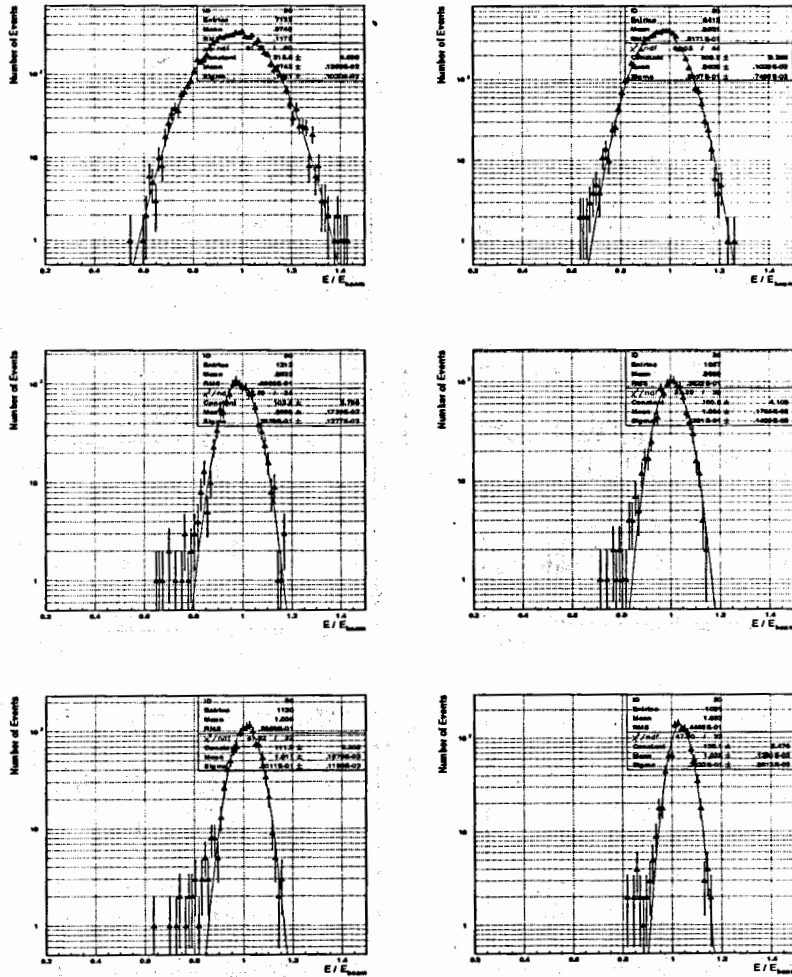
Figure 6: The normalized electron response (E_e/E_{beam}) for E = 10, 60, 100 GeV (left column, up to down) and E = 20, 80, 180 GeV (right column, up to down) at $\eta = -0.55$.
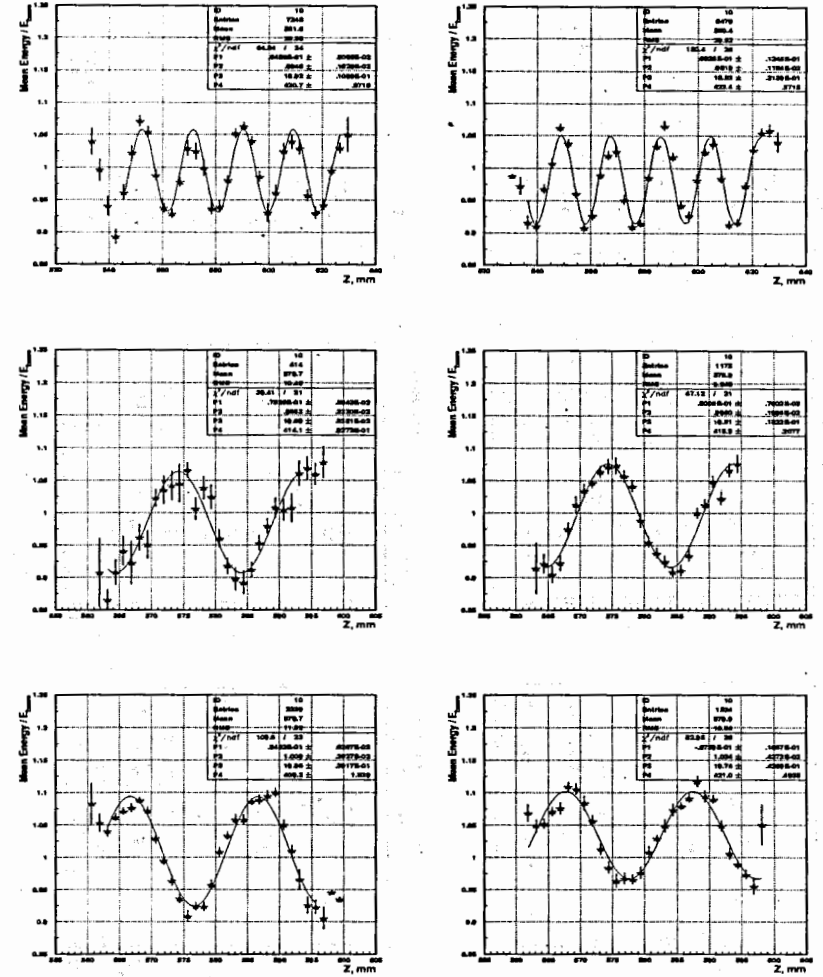
Figure 7: The normalized electron response (E_e/E_{beam}) for E = 10, 60, 100 GeV (left column, up to down) and E = 20, 80, 180 GeV (right column, up to down) at $\eta = -0.25$ as a function of impact point Z coordinate.
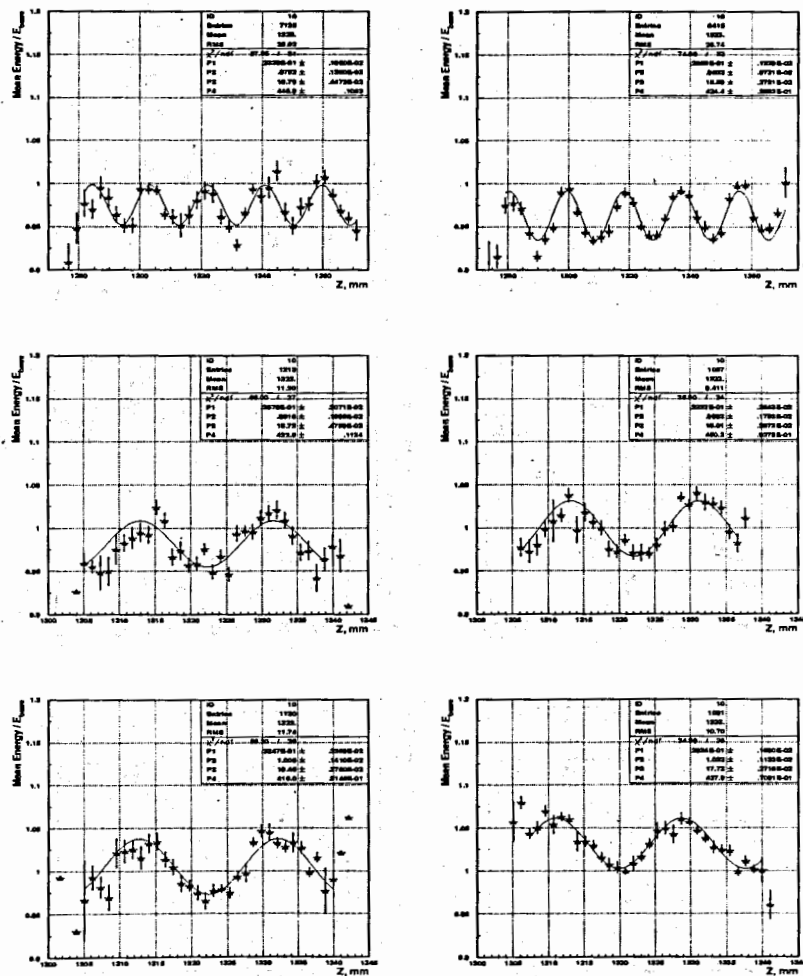
Figure 8: The normalized electron response (E_e/E_{beam}) for E = 10, 60, 100 GeV (left column, up to down) and E = 20, 80, 180 GeV (right column, up to down) at $\eta = -0.55$ as a function of impact point Z coordinate.
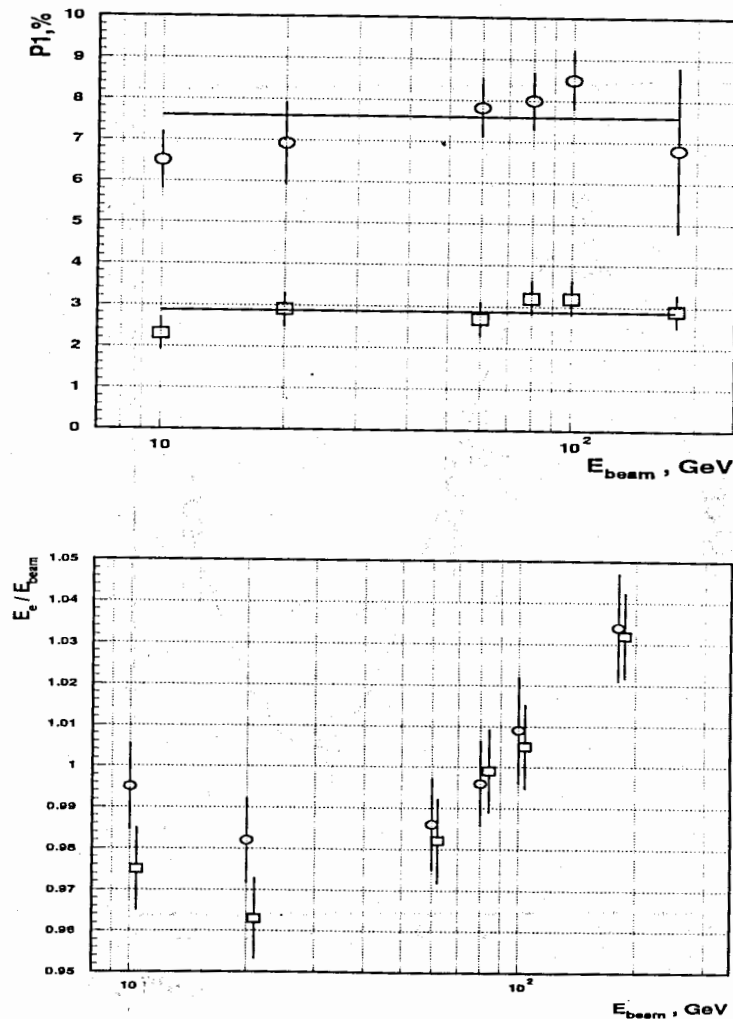
Figure 9: Top: The amplitude (parameter P_1) of the electron response as a function of the beam energy. Bottom: The mean normalized electron response as a function of the beam energy. $\bigcirc$ ($\square$) are the data for $\eta = -0.25$ (-0.55).
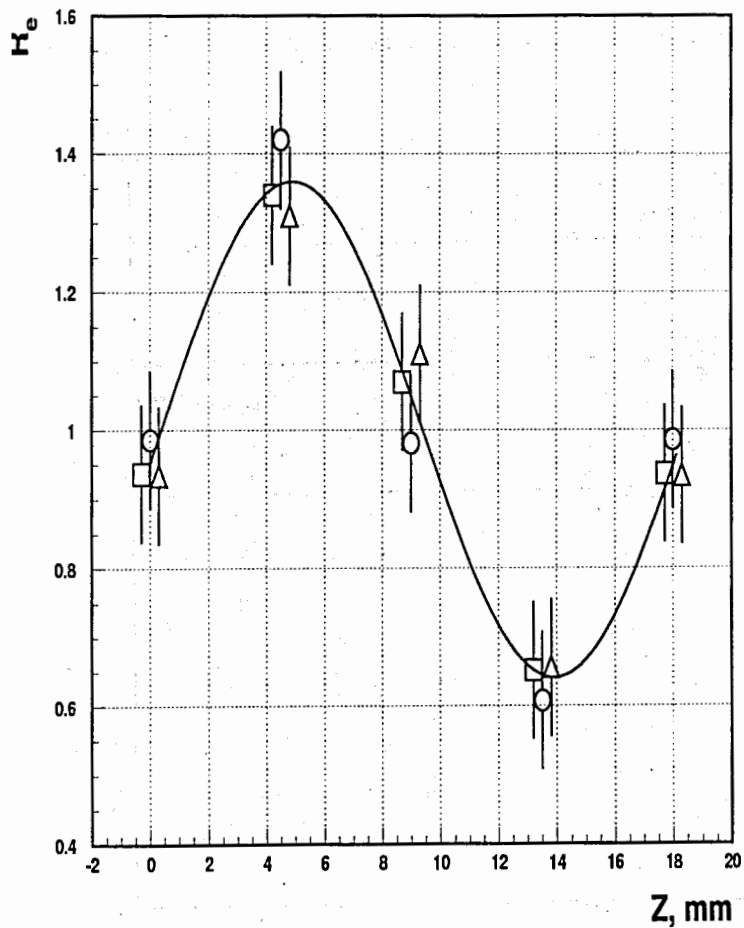
Figure 10: The electron response as a function of Z coordinate (calculations). $\bigcirc$ are for 10 GeV energy, $\square$ are for 100 GeV energy, $\triangle$ are for 100 GeV energy.
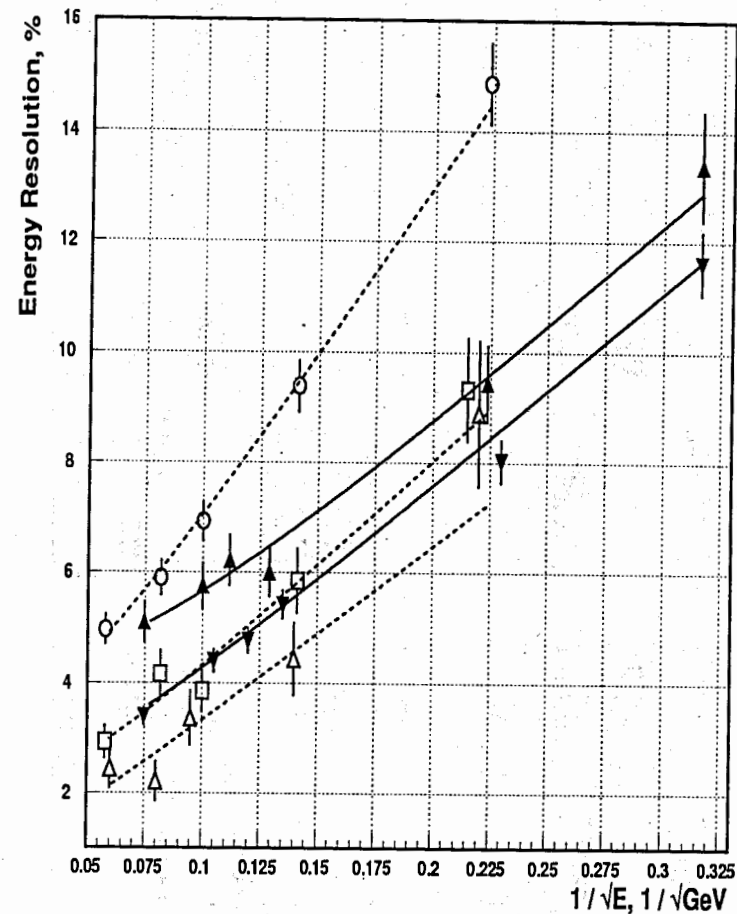
Figure 11: The energy resolution for electrons as a function of energy. The black points are the Module-0 data ($\blacktriangle$ are the 14° data, $\blacktriangledown$ are the 30° data), the open points are the 1m prototype modules data ($\bigcirc$ – 10°, $\square$ – 20°, $\triangle$ – 30°). The lines are fits of eq. (5).
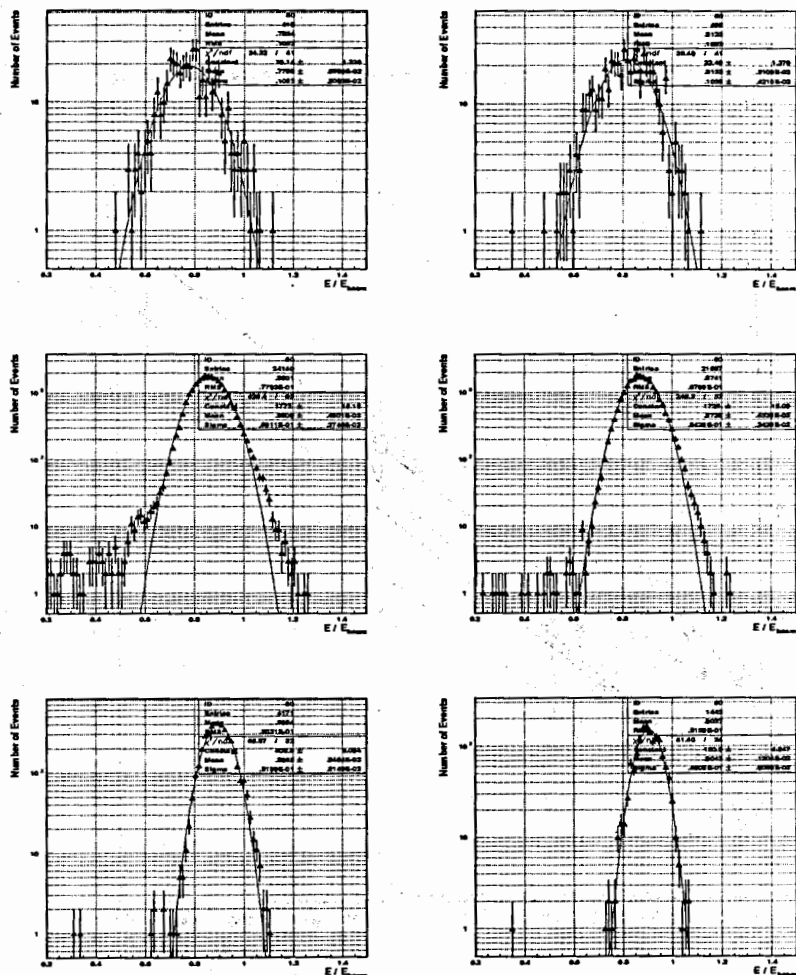
Figure 12: The distributions of the normalized pion response (E_π/E_{beam}) for E = 20, 100, 180 GeV at $\eta = -0.25$ (left column, up to down) and at $\eta = -0.55$ (right column, up to down).

Figure 13: The normalized pion response (E_π/E_{beam}) for $E_{beam} = 20$, 100, 180 GeV at $\eta = -0.25$ (left column, up to down) and at $\eta = -0.55$ (right column, up to down) as a function of Z coordinate.
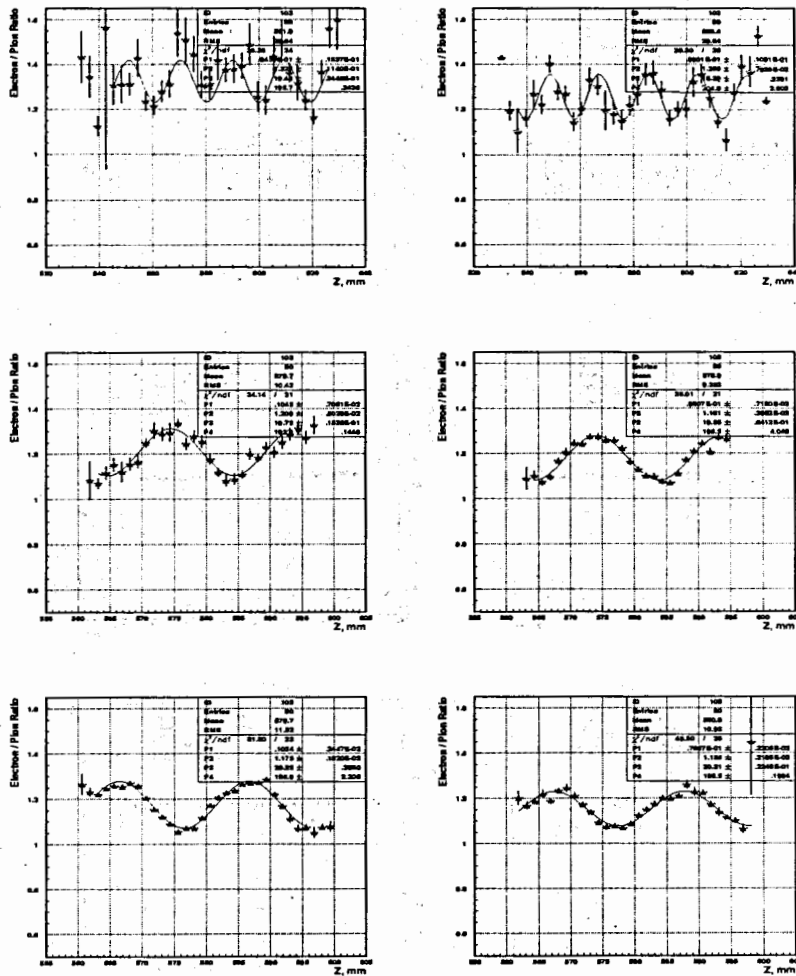
Figure 14: The e/π ratio for Module-0 as a function of Z coordinate for E = 10, 60, 100 GeV (left column, up to down) and E = 20, 80, 180 GeV (right column, up to down) at $\eta = -0.25$.
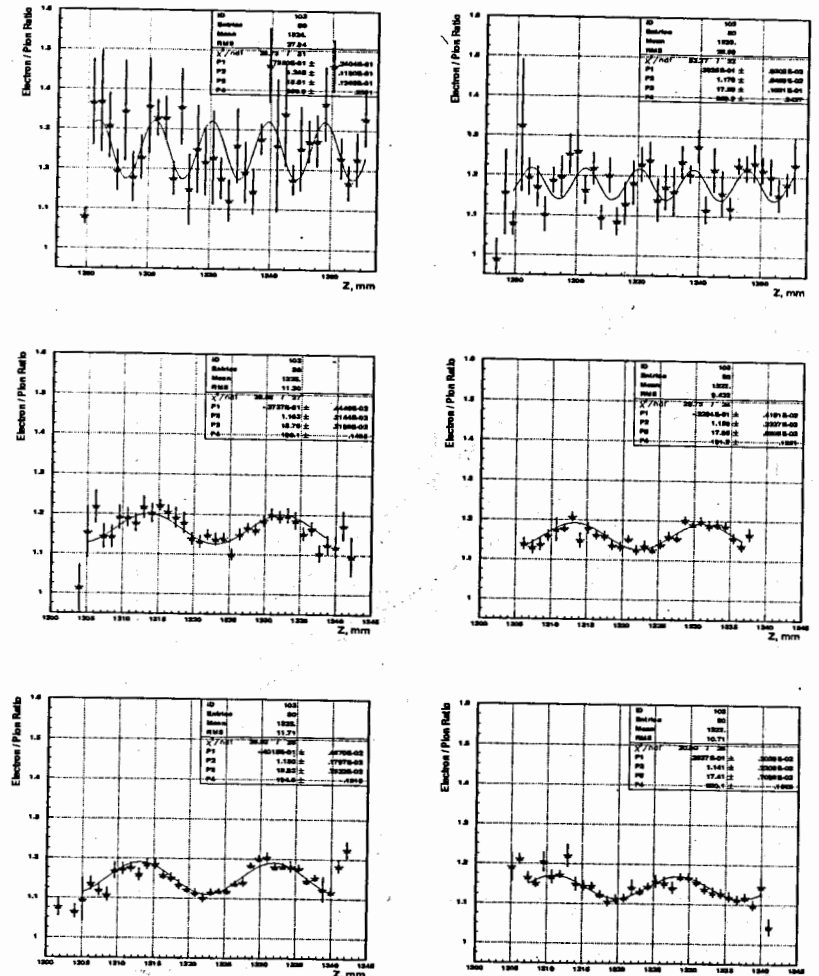
Figure 15: The e/π ratio for the Module-0 as a function of Z coordinate for E = 10, 60, 100 GeV (left column, up to down) and E = 20, 80, 180 GeV (right column, up to down) at $\eta = -0.55$.
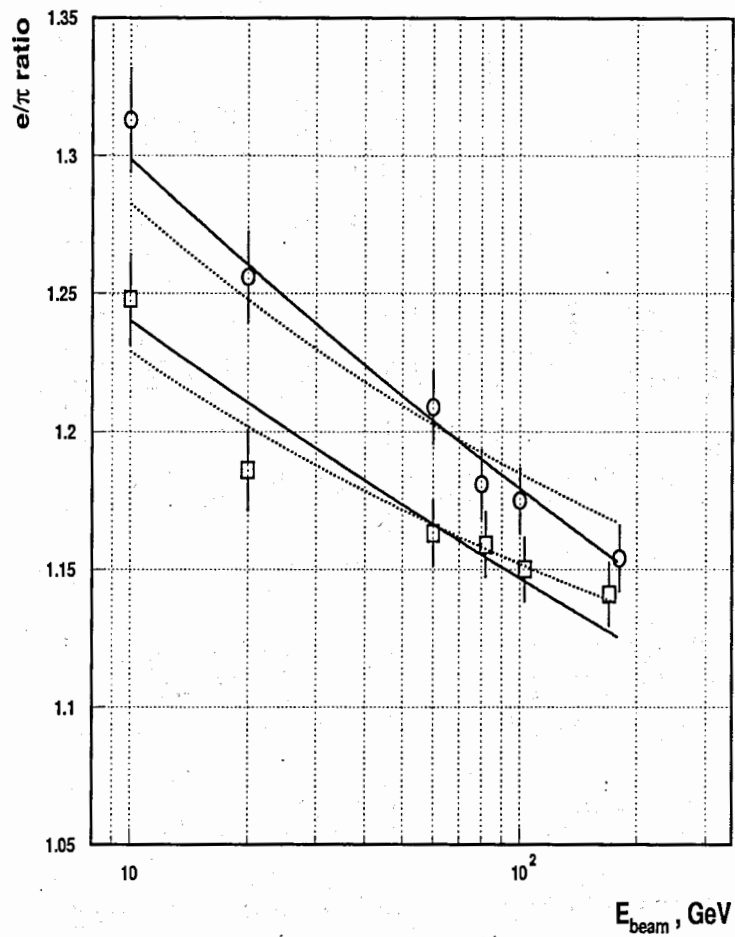
Figure 16: The e/π ratio as a function of the beam energy for the Module-0: the ∘ points are the $\eta = -0.25$ data, the □ points are the $\eta = -0.55$ data. The solid (dashed) lines are the fits of equation (7) with the Wigmans (Groom) parameterization of $f_{\pi^\circ}(E)$.
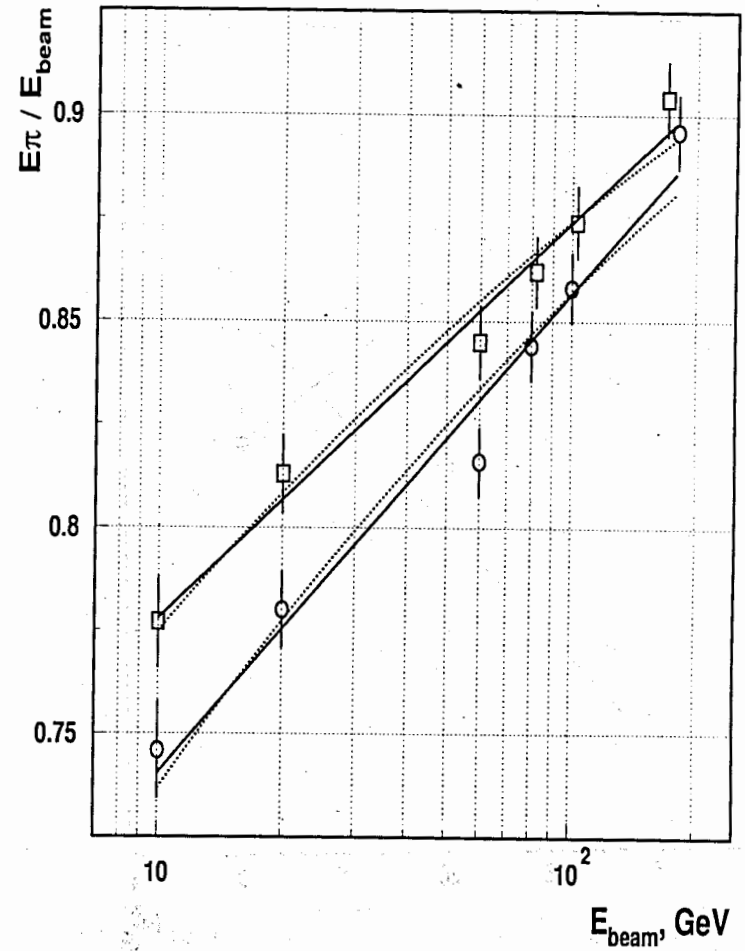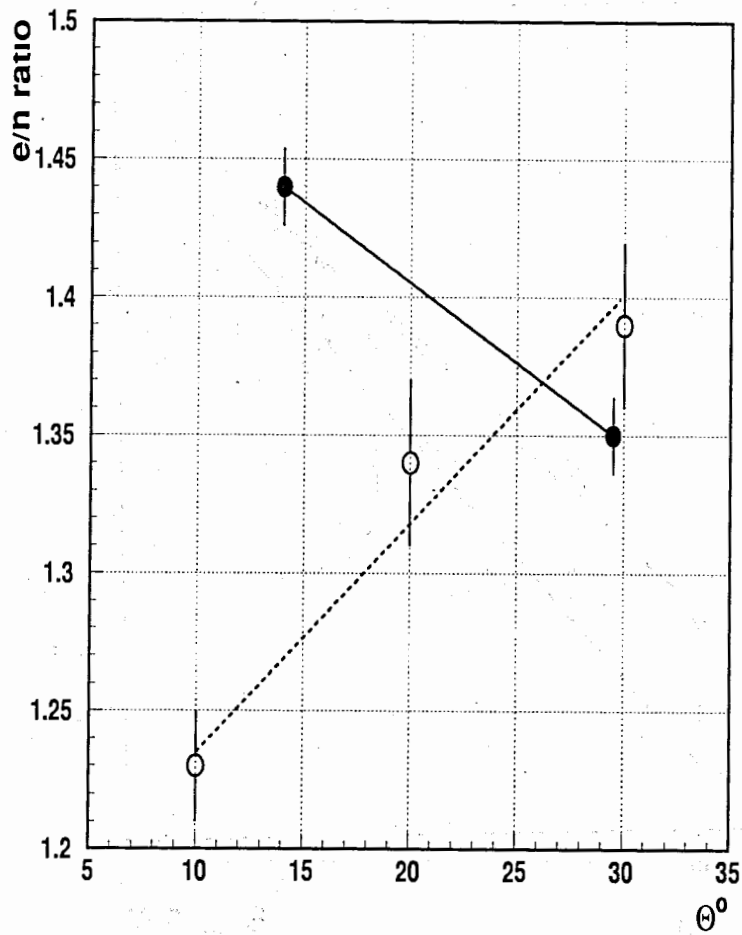

Figure 17: The mean normalized pion response (E_π/E_{beam}) as a function of the beam energy for the Module-0: the ∘ points are the $\eta = -0.25$ data, the □ points are the $\eta = -0.55$ data. The solid (dashed) lines are the fits of equation (7) with the Wigmans (Groom) parameterization of $f_{\pi^\circ}(E)$.

Figure 18: The e/h ratios for the Module-0 (black points) and the 1m propotype modules (open points) as a function of Θ angle.
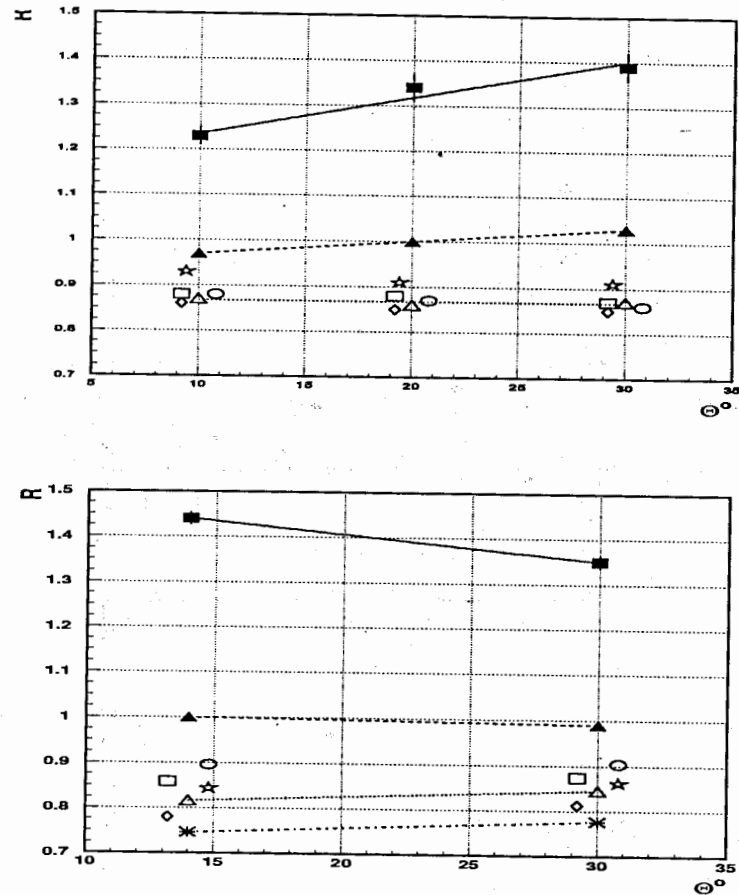

Figure 19: Top: The e/h ratios, the electron and pion responses for the 1m propotype modules as a function of Θ angle. ■ are the e/h ratios, ▲ are the electron response, the rest is the pion response for 20 (◇), 50 (△), 100 (□), 150 (○), 300 (⋆) GeV. Bottom: The e/h ratios, the electron and pion responses for the Module-0 as a function of Θ angle. ■ are the e/h ratios, ▲ are the electron response, the rest is the pion response for 10 (∗), 20 (◇), 60 (△), 80 (⋆), 100 (□), 180 (○) GeV. The lines are the results of linear fits.
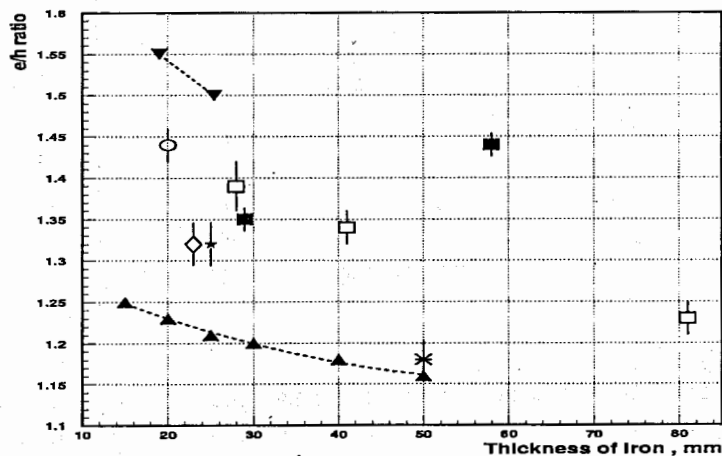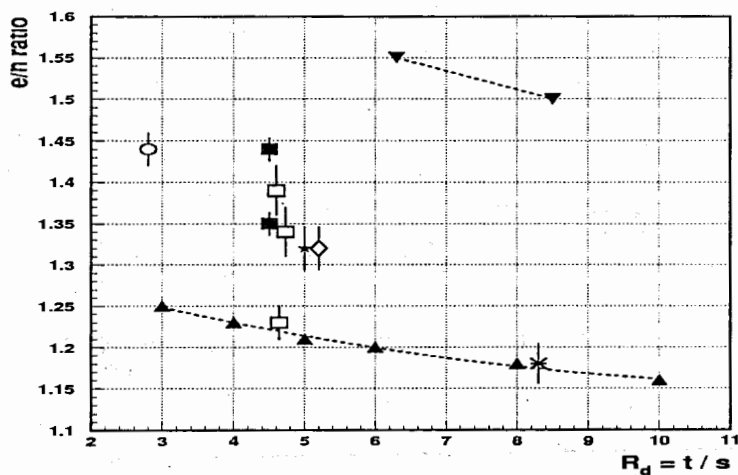
Figure 20: Top: The e/h-ratios as a function of R_d. Bottom: The e/h-ratios as a function of iron thickness.

9 Conclusions

The detailed experimental information about the electron and pion responses, the electron energy resolution and the e/h ratios as a function of the incident energy E, the impact point Z and the incidence angle Θ of the Module-0 of the ATLAS iron-scintillator barrel hadron calorimeter with the longitudinal tile configuration is obtained. The results are compared with the existing experimental data, obtained for the 1m prototype modules and the various iron-scintillator calorimeters, and with the Monte Carlo calculations. It is shown that the e/h ratio has very complicated behaviour being the function of the thickness of the passive (iron) layers, the sampling fraction and, in our case, from the Θ angle and the sizes and replacement of the scintillator tiles.

10 Acknowledgments

References

[1] ATLAS Collaboration, ATLAS Technical Proposal for a General-Purpose pp Experiment at the Large Hadron Collider, CERN/ LHCC/ 94-93, CERN, Geneva, Switzerland, 1994.

[2] LHC News, $N^{\underline{o}}$ 7 September 1995, CERN, Geneva, Switzerland.

[3] O. Gildemeister, F. Nessi-Tedaldi and M. Nessi, Proc. 2nd Int. Conf. on Cal. in HEP, Capri, 1991.

[4] ATLAS Collaboration, ATLAS TILE Calorimeter Technical Design Report, CERN/ LHCC/ 96-42, ATLAS TDR 3, CERN, Geneva, Switzerland, 1996.

[5] J.A. Budagov, Y.A. Kulchitsky, V.B. Vinogradov et al., JINR, E1-95-513, Dubna, Russia, 1995; ATLAS Internal note, TILECAL-No-72, CERN, Geneva, Switzerland, 1995.

[6] E. Berger et. al., CERN/LHCC 95-44, CERN, Geneva, Switzerland.

[7] F. Ariztizabal et. al., NIM A349 (1994) 384.

[8] A. Juste, ATLAS Internal note, TILECAL-No-69, 1995, CERN, Geneva, Switzerland.

[9] G. Abshire et. al., NIM 164 (1979) 67.

[10] J. Del Peso, E. Ros, NIM A276 (1989) 456.

[11] D. Groom, Proceedings of the Workshop on Calorimetry for the Supercollides, Tuscaloosa, Alabama, USA, 1990.

[12] R. Wigmans, NIM A265 (1988) 273.

[13] R. Wigmans, NIM A259 (1987) 389.

[14] T. A. Gabriel et. al., NIM A295 (1994) 336.

[15] S. L. Stone et. al., NIM 151 (1978) 387.

[16] Y. A. Antipov et. al., NIM 180 (1990) 81.

[17] H. Abramowicz et. al., NIM 180 (1981) 429.

[18] V. Bohmer et. al., NIM 122 (1974) 313.

[19] M. De Vincenze et. al., NIM A243 (1986) 348.

[20] M. Holder et. al., NIM 151 (1978) 69.